2019 American Control Conference (ACC)
Philadelphia, PA, USA, July 10-12, 2019

Estimating Rack Force due to Road Slopes for Electric Power Steering Systems

Akshay Bhardwaj[1], Brent Gillespie[1], James Freudenberg[2]

Abstract— **The net force generated by tire moments on the steering rack of a vehicle, called the rack force, holds a significant amount of information about the tire-road angle, the surface profile of road, and the speed of the vehicle. As a result, many electric power steering control applications rely on the estimation of rack force. Current methods of rack force estimation are inaccurate because they either do not account for road profile in the rack force estimation or are susceptible to disturbances acting in the steering system. In this paper we overcome both of these limitations and develop two real-time capable models to estimate the rack force for driving on longitudinal and lateral road slopes using vehicle and tire dynamics models. We demonstrate the accuracy of our models by analyzing the results from actual driving experiments performed on sloped roads under normal and aggressive driving situations. We also compare the performance of the two models with a model existing in the literature that does not account for road slopes.**

Index Terms— **Rack Force, Road Slopes, Vehicle Dynamics, Electric Power Steeering**

I. INTRODUCTION

The torque experienced by a driver at the steering wheel plays an important role in lateral control of a vehicle. Although visual information may be the predominant feedback modality to support driving manoeuvres, torque feedback at the steering wheel couples the driver's hands and arms to the vehicle and is essential for smooth and controlled vehicle lateral response [1]. Electric power steering (EPS) systems can regulate this torque feedback to enhance driver comfort and safety. The primary role of EPS is to generate an assist torque to reduce the driver's steering effort based on the measurements of steering torque [2]. However, with the development of advanced driver assist functions and increasing autonomy in vehicles, the role of EPS is slowly changing. Now, apart from performing its usual function of reducing the driver's steering effort, EPS is being used to realize advanced steering controllers that enhance the steering feel. The fundamental objective of such controllers is to provide the driver an accurate display of tire-road interaction while reducing steering effort, removing disturbances, and improving the quality of steering feedback [1], [3]–[5]. Literature suggests that these requirements can be met if the EPS assist torque is not only generated on the basis of the steering torque but is also generated on the basis of the force acting on the steering rack [1]–[3]. This force, called the rack force, is generated through tire-road interaction forces and moments that result from steering angle, vehicle speed and road profile variations such as longitudinal road slopes (road grades), lateral road slopes (road banks), side-slopes etc. While the steering angle and vehicle speed have been used in the past to estimate the rack force, the road profile variation has been ignored [3], [6]. The focus of this paper is to fill this gap and develop models that can account for road profile variations in rack force estimation.

Rack force estimates have been used in designing steering feedback in driving simulators, hardware in the loop simulators [6], [7], disturbance rejection controllers [1], [3], [8], lane keeping assist systems, road friction estimators, steer-by-wire position controllers [5], [7], and in performing steering system evaluation and bench-marking [9]. The most common method to calculate rack force available in the literature is based on an input observer that uses sensors and a lumped parameter model of the steering system [1], [5], [7], [8], [10]. The rack force estimates produced by this method are accurate in most driving situations including driving on varying road profiles. However, as shown in [1], [3], the estimates are susceptible to steering system disturbances that can arise due to manufacturing asymmetries, wear and tear, and misalignments in wheels, suspension, and steering system components. Another method to estimate the rack force suggested in the literature is based on identifying a model for rack force based on test data using system identification techniques [8], [9]. In [9], a rack force model is identified by characterizing a relationship between the physical measurements of the output rack force and input rack displacement from actual vehicle test data. A limitation of such models is in their limited applicability in maneuvers and vehicle configurations different from the ones for which they are identified. Also, like the observer-based method, there is no guarantee that the identified models are insusceptible to disturbances.

In this paper, we propose the use of physics-based tire and vehicle dynamics models to determine the steering rack force based on sensed (or estimated) road inputs (such as slope angles), vehicle speed, and steering angle. By using only the primary inputs that directly affect the tire forces we circumvent the presence of undesired disturbances in the rack force estimates. A few groups in the past ([1], [3], [6], [11]) have used vehicle dynamics models for rack force estimation but all of them ignored the presence of road profile variations. As a first step towards modeling the effect of road profile on the rack force, in this paper, we present vehicle

*This work was supported by Ford Motor Company

[1] are with the Department of Mechanical Engineering, University of Michigan, Ann Arbor, Michigan 48105, USA (akshaybh,brentg)@umich.edu

[2] is with the Department of Electrical & Computer Engineering, University of Michigan, Ann Arbor, Michigan 48105, USA jfr@umich.edu

dynamic models that can account for road slope variations in rack force estimation. We develop two dynamic models of which one has higher fidelity and complexity than the other. Then we present the results from actual driving tests for different road slopes and compare the relative accuracies of the two models using real-time measurements from a rack force sensor. Furthermore, we compare the sensed rack force and the rack force estimated using our models with the estimates of a model existing in the literature that does not account for road slopes [1].

II. Modeling Framework

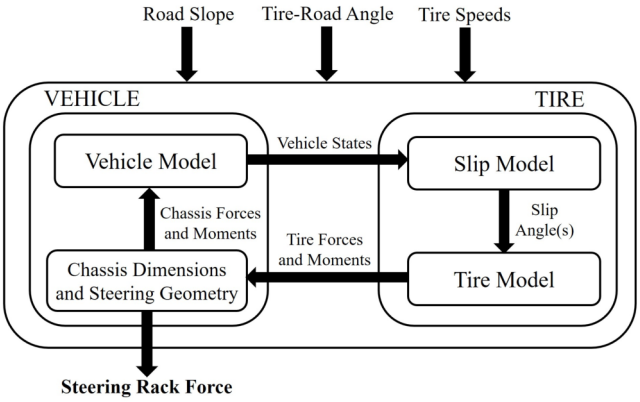

Fig. 1: A communicating vehicle model and tire model enable the estimation of rack force given road slope, tire-road angle, and tire speed inputs.

Figure 1 describes a dynamic model for estimating the steering rack force. Three inputs are required in the model; namely, either lateral road slope θ or longitudinal road slope θ_l, tire-road angle δ, and tire speeds Ω. Of these, tire-road angle δ and tire speeds Ω are available through steering angle and wheel speed sensors while road slopes were estimated in real time so that the model does not use the sensors on the top of those that were available in the vehicle. In particular, vehicle's acceleration (lateral a_y and longitudinal a_x), longitudinal speed u, and yaw rate $\dot{\psi}$ sensed using on-board accelerometers, wheel speed sensors, and rate gyros respectively were used to estimate the lateral slope θ and longitudinal slope θ_l using the following equations

$$\theta = \arcsin\left(\frac{a_y - u\dot{\psi}}{g}\right) \tag{1}$$

$$\theta_l = \arcsin\left(\frac{a_x - \dot{u}}{g}\right) \tag{2}$$

The derivations of these equations can be found in [12]. The longitudinal velocity u is calculated by multiplying the rear tire speeds and tire rolling circumferences and averaging the two resulting products.

Using these inputs, a dynamic model of the vehicle is required to generate the vehicle states (lateral speed, yaw rate, roll angle, etc.) that are fed into a tire slip model which in turn determines the slip angles of the tire. Normal tire forces are adjusted according to the road slope value, and along with the slip angles, are used as primary inputs in a tire model. The tire model computes the forces and moments acting on the tire. The tire forces and moments are then transformed to the vehicle-fixed coordinate frame using vehicle states and chassis dimensions, which, along with the non-vertical component of the vehicle's weight due to road slope, are used as inputs to the vehicle model to generate the states for the next time interval. During this process, the aligning moments resulting from the tire model are used to determine the steering rack force (using information of the transmission mechanics of tire moments to rack force).

Two dynamic models were developed: A 2 degree of freedom bicycle model with a simple brush tire model based on lateral tire slip (2 DOF Model) [13], and a 3 degree of freedom 4-wheel vehicle model with an extended brush tire model based on combined longitudinal and lateral slip (3 DOF Model) [14]. Both models were designed for front wheel steered vehicles and for lateral road slopes. In addition, dynamic equations for longitudinal slopes are presented. Different versions of the presented 2DOF vehicle model for modeling vehicle dynamics due to lateral road slope and longitudinal road slope already exist in the literature (for example [15], [16]). However, the developed 3DOF vehicle model for the lateral and longitudinal road slopes is novel and has not appeared in the literature to the best of our knowledge. In the following sections, we briefly discuss the development of these two models.

III. 2DOF Model

A. Vehicle Model

Figure 2 shows the definition of frames for a bicycle model driving on a road (with lateral slope θ) with a yaw angle ψ measured with respect to a unit vector fixed on the road. Frame A is fixed on the ground and is considered Newtonian. Frame B is fixed on the road and is obtained by rotating frame A through the angle θ (slope angle) about $\hat{i}_A$. Since the slope of the road changes slowly we can assume that frame B is also Newtonian. Frame C is attached to the vehicle chassis and is obtained by rotating frame B through angle ψ around $\hat{k}_B$. The longitudinal speed u and lateral speed v of the vehicle are defined in frame C. The road wheel angle is denoted by δ. The center of gravity c of the vehicle is located at (x, y) in frame B. The height of c above the ground in direction $\hat{k}_B$ is denoted by h and is measured as the distance between point c and a point a on the ground that is fixed in the vehicle frame. The distance between the center of the front tire contact patch and the point a is l_f and between the center of the rear tire contact patch and point a is l_r. The position vector of the center of gravity c, and angular velocity of the vehicle with respect to frame B are given by

$$\vec{r}_{c/o} = h\hat{k}_B + x\hat{i}_B + y\hat{j}_B \qquad \vec{\omega}_{C/B} = \dot{\psi}\hat{k}_C$$

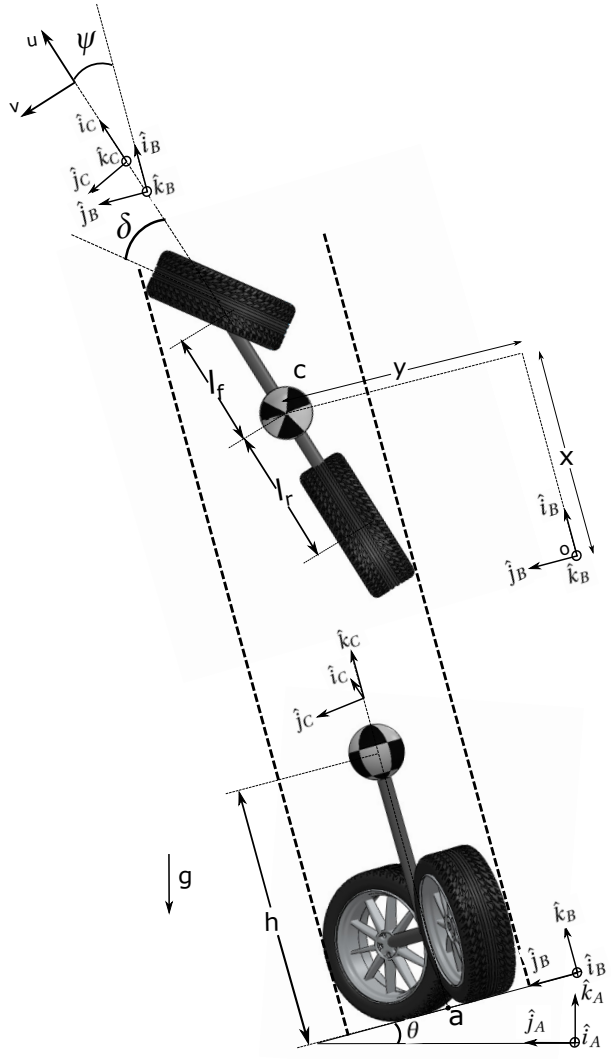

Fig. 2: A 2DOF bicycle model drives on a road with lateral slope θ, where θ is a rotation about vector $\hat{i}_A$. In the configuration shown, the vehicle is headed down the slope at an angle ψ with respect to the vector $\hat{k}_B$ and has a steering angle δ. The upper view shows the projection of the vehicle onto the road. The lower view shows the vehicle projected onto a plane perpendicular to $\hat{i}_A$.

the speed of point c resolved in the road-fixed and vehicle-fixed frames and corresponding acceleration are given by

$$\vec{v}_{c/o} = \dot{x}\hat{i}_B + \dot{y}\hat{j}_B = u\hat{i}_C + v\hat{j}_C.$$
$$\vec{a}_{c/o} = (\dot{u} - v\dot{\psi})\hat{i}_C + (\dot{v} + u\dot{\psi})\hat{j}_C$$

The net forces acting on the vehicle center of gravity c due to tire forces in all three directions ($F_{x,n}$, $F_{y,n}$, $F_{z,n}$) and due to the gravitational force can be written as

$$\vec{F}_{net} = F_{x,n}\hat{i}_C + (F_{y,n} - mg\sin\theta)\hat{j}_C + (F_{z,n} - mg\cos\theta)\hat{k}_C$$

From Newton's second law $m\vec{a}_{c/o} = \vec{F}_{net}$, we obtain longitudinal and lateral translational dynamics equations as

$$m\dot{u} - mv\dot{\psi} = F_{x,n} \;;\; m\dot{v} + mu\dot{\psi} + mg\sin\theta = F_{y,n} \quad (3)$$

Likewise, for a bicycle model driving on longitudinal slope θ_l, the following equations of motion can be obtained

$$m\dot{u} - mv\dot{\psi} + mg\sin\theta_l = F_{x,n} \;;\; m\dot{v} + mu\dot{\psi} = F_{y,n} \quad (4)$$

We now derive the rotational dynamics for the vehicle. Assuming symmetry about the X-Y and Y-Z planes of the vehicle, the inertia matrix of the vehicle V with respect to point c resolved in frame C is given by

$$\vec{I}_{V/c}|_C = \begin{bmatrix} I_{xx} & 0 & -I_{xz} \\ 0 & I_{yy} & 0 \\ -I_{xz} & 0 & I_{zz} \end{bmatrix}, \quad (5)$$

where I_{xx}, I_{yy}, and I_{zz} are the moments of inertia about the unit vectors of frame C and I_{xz} is a product of inertia. Euler's equation for rotation of the vehicle [17] with angular speed $\vec{\omega}_{C/B}$ and angular acceleration $\vec{\alpha}_{C/B}$ gives

$$\vec{I}_{V/c}\vec{\alpha}_{C/B} + \vec{\omega}_{C/B} \times \vec{I}_{V/c}\vec{\omega}_{C/B} = \vec{M}_{V/c}$$

$$I_{zz}\ddot{\psi} = M_{V/c}, \quad (6)$$

where $M_{V/c}$ is the net moment on the vehicle about point c. Denoting tire forces on the front and rear tires in longitudinal and lateral directions respectively by F_{xf}, F_{xr} and F_{yf}, F_{yr}, the net forces and moments acting on the vehicle center of gravity c due to the tire forces can be given by

$$F_{x,n} = F_{xf}\cos\delta - F_{yf}\sin\delta + F_{xr}$$
$$F_{y,n} = F_{xf}\sin\delta + F_{yf}\cos\delta + F_{yr}$$
$$M_{V/c} = l_f F_{xf}\sin\delta + l_f F_{yf}\cos\delta - l_r F_{yr}$$

Since the longitudinal speed u of the vehicle is an input, the two degrees of freedom, namely, lateral speed v and yaw rate $\dot{\psi}$ are modeled using equations (3) and (6)

$$m\dot{v} + mu\dot{\psi} + mg\sin\theta = F_{xf}\sin\delta + F_{yf}\cos\delta + F_{yr} \quad (7)$$

$$I_{zz}\ddot{\psi} = l_f F_{xf}\sin\delta + l_f F_{yf}\cos\delta - l_r F_{yr} \quad (8)$$

For longitudinal slope, the equations are given by

$$m\dot{v} + mu\dot{\psi} = F_{xf}\sin\delta + F_{yf}\cos\delta + F_{yr} \quad (9)$$
$$I_{zz}\ddot{\psi} = l_f F_{xf}\sin\delta + l_f F_{yf}\cos\delta - l_r F_{yr} \quad (10)$$

B. Tire and Slip Models

Using the states obtained from the 2DOF vehicle model, the lateral slip angles α_f and α_r of the front and rear tires respectively were obtained using the expressions given in [13]. The lateral force on the front and rear tires with respective cornering stiffness C_{α_f} and C_{α_r} and aligning moment M_z for the front tire are then given by

$$F_{yf} = C_{\alpha_f}\alpha_f; \quad F_{yr} = C_{\alpha_r}\alpha_r; \quad M_z = F_{yf}(t_p + t_m), \quad (11)$$

where the mechanical trail t_m is a constant for the test vehicle, and pneumatic trail of the tire is given in [13].

For the road slope θ (lateral or longitudinal), the normal force on the front tire is

$$F_{zf} = \frac{mgl_r \cos\theta}{2(l_f + l_r)}. \tag{12}$$

The steering rack force is simply given by

$$F_R = i_p M_z,$$

where the constant ratio i_p defines the tire moment to rack force transmission ratio for the test vehicle. The parameters for the 2DOF model are specified in Table I.

Parameter	Value
h	0.6 m
m	1972 kg
I_{zz}	3600 kg m^2
l_f	1.19 m
l_r	1.69 m

Parameter	Value
$C_{\alpha f}$	136 kN/rad
$C_{\alpha r}$	136 kN/rad
t_m	0.0313 m
μ	1
i_p	7.03 m^{-1}

TABLE I: 2DOF model parameters

C. 2DOF Model Assembly

We now refer back to Fig. 1. The vehicle states, namely, lateral speed v and yaw rate $\dot{\psi}$ are modeled using equation (7) and (8). The lateral speed v and yaw rate $\dot{\psi}$ are used to find the tire lateral slip angles [13]. Slip angles are used to find the tire forces and aligning moments using equation (11). The tire forces are fed back in the vehicle model in equation (7) and equation (8) to generate the vehicle states for the next time sample.

IV. 3DOF Model

A. Vehicle Model

Figure 3 shows the definitions of frames for the double track model of a vehicle with four wheels. The frames A, B, C, point a, and point c and its location are defined in the same way as defined in figure 2. However, in this model, frame C is attached to the unsprung mass of the vehicle chassis and frame D is attached to the vehicle chassis (sprung mass) and is obtained by rotation of frame C around $\hat{i}_C$ by the additional degree of freedom ϕ, that is the vehicle roll angle. The height of the roll axis ($\hat{i}_C$) above ground is denoted by h_2 and is measured along $\hat{k}_B$ as the distance between point b and point a. The height of the sprung mass h_1 is defined as the distance between the center of gravity c and point b on the roll axis. The track width for the front axle is given by $2t_f$ and the track width for the rear axle is given by $2t_r$.

The angular velocity of the vehicle with respect to ground, and the position and velocity of c are given by

$$\vec{\omega}_{D/B} = \dot{\phi}\hat{i}_D + \dot{\psi}\sin\phi\hat{j}_D + \dot{\psi}\cos\phi\hat{k}_D \tag{13}$$

$$\vec{r}_{c/o} = h_1\hat{k}_D + h_2\hat{k}_C + x\hat{i}_B + y\hat{j}_B$$

$$\vec{v}_{c/o} = (u + h_1\dot{\psi}\sin\phi)\hat{i}_C + (v - h_1\dot{\phi}\cos\phi)\hat{j}_C - h_1\dot{\phi}\sin\phi\hat{k}_C \tag{14}$$

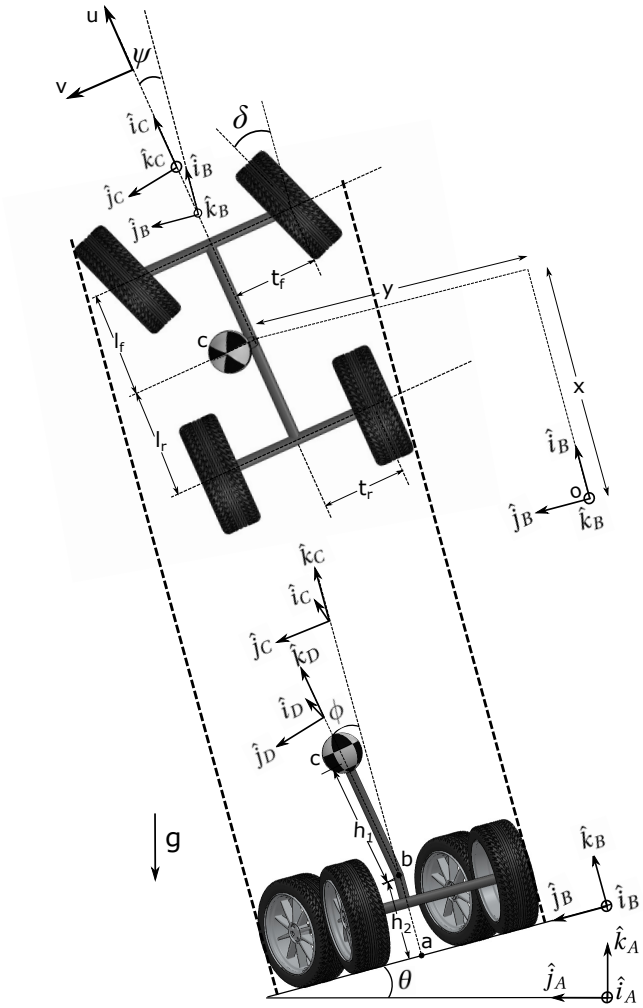

Fig. 3: A 3DOF bicycle model drives on a road with lateral slope θ, where θ is a rotation about vector $\hat{i}_A$. In the configuration shown, the vehicle is headed down the slope at an angle ψ with respect to the vector $\hat{k}_B$ and has a steering angle δ. The vehicle chassis is shown with a roll angle ϕ about the vector $\hat{i}_C$. The upper view shows the projection of the vehicle onto the road. The lower view shows the vehicle projected onto a plane perpendicular to $\hat{i}_A$.

Using equations (5), (13), and (14), the net resulting kinetic energy [17] of the vehicle V with respect to a point o on ground in the Newtonian Frame B is given by

$$K_{V/o/B} = \frac{1}{2}(I_{xx}\dot{\phi}^2 + I_{yy}\dot{\psi}^2\sin^2\phi + I_{zz}\dot{\psi}\cos^2\phi - 2I_{xz}\dot{\psi}\dot{\phi}\cos\phi + \frac{1}{2}m((u + h_1\dot{\psi}\phi)^2 + (v - h_1\dot{\phi}\cos\phi)^2 + (h_1\dot{\phi}\sin\phi)^2)$$

Representing the suspension springs and antiroll bars by front and rear roll stiffnesses $c_{\phi 1}$ and $c_{\phi 2}$ respectively, and the damping in the wheel suspensions by coefficients $k_{\phi 1}$ and

$k_{\phi 2}$ [14], the total potential energy [17] of the vehicle reads

$$U_V = mgh_1 \sin\phi \sin\theta \sin\psi + mg(h_1 \cos\phi + h_2)\cos\theta + mgy \sin\theta + \frac{1}{2}c_{\phi 1}\phi^2 + \frac{1}{2}c_{\phi 2}\phi^2$$

To obtain the equations of motion, we solved Lagrange's equation for the vehicle V described by generalized coordinates q_i and generalized forces and moments Q_i [17]

$$\frac{d}{dt}\frac{\partial K_{V/o/B}}{\partial \dot{q}_i} - \frac{\partial K_{V/o/B}}{\partial q_i} + \frac{\partial U_V}{\partial q_i} = Q_i,$$

where x, y, ψ, ϕ were chosen as the generalized coordinates in q_i. Assuming that roll angle ϕ and $\dot{\phi}$ remain small, the equations of motion are given as

$$m\dot{v} + m\dot{\psi}u - mh_1\ddot{\phi} + mh_1\dot{\psi}^2\phi + mg\sin\theta = Q_v \quad (15)$$

$$(I_{zz}(1-\phi^2) + (I_{yy} + mh_1^2)\phi^2)\ddot{\psi} - I_{xz}\ddot{\phi} + 2(I_{yy} - I_{zz} + mh_1^2)\dot{\psi}\dot{\phi}\phi + mh_1(\dot{u} - \dot{\psi}v)\phi + mgh_1\phi\cos\psi\sin\theta = Q_\psi \quad (16)$$

$$(I_{xx} + mh_1^2)\ddot{\phi} - mh_1(\dot{v} + \psi u) - I_{xz}\dot{\psi} - (I_{yy} - I_{zz} + mh_1^2)\dot{\psi}^2\phi + (c_{\phi 1} + c_{\phi 2})\phi - mgh_1 (\phi\cos\theta - \sin\psi\sin\theta) = Q_\phi \quad (17)$$

Similarly, for longitudinal slope θ_l, the following equations were obtained

$$m\dot{v} + m\dot{\psi}u - mh_1\ddot{\phi} + mh_1\dot{\psi}^2\phi = Q_v \quad (18)$$

$$(I_{zz}(1-\phi^2) + (I_{yy} + mh_1^2)\phi^2)\ddot{\psi} - I_{xz}\ddot{\phi} + 2(I_{yy} - I_{zz} + mh_1^2)\dot{\psi}\dot{\phi}\phi + mh_1(\dot{u} - \dot{\psi}v)\phi - mgh_1\phi\cos\psi\sin\theta_l = Q_\psi \quad (19)$$

$$(I_{xx} + mh_1^2)\ddot{\phi} - mh_1(\dot{v} + \psi u) - I_{xz}\dot{\psi} - (I_{yy} - I_{zz} + mh_1^2)\dot{\psi}^2\phi + (c_{\phi 1} + c_{\phi 2})\phi - mgh_1 (\phi\cos\theta_l + \sin\psi\sin\theta_l) = Q_\phi, \quad (20)$$

where the generalized forces are given by

$$Q_v = F_{y1,V} + F_{y2,V} + F_{y3,V} + F_{y4,V}$$
$$Q_\psi = M_{z1} + M_{z2} + M_{z3} + M_{z4} + F_{x1,V}t_f + F_{y1,V}l_f - F_{x2,V}t_f + F_{y2,V}l_f + F_{x3,V}t_r - F_{y3,V}l_r - F_{x4,V}t_r - F_{y4,V}l_r$$
$$Q_\phi = -(k_{\phi 1} + k_{\phi 2})\dot{\phi},$$

and subscripts 1, 2, 3, and 4 denote the front right, front left, rear right, and rear left tires respectively. The longitudinal and lateral forces $F_{xi,V}$, $F_{yi,V}$ acting on the vehicle due to the tires are given by

$$\begin{aligned} F_{xi,V} &= F_{xi}\cos\delta - F_{yi}\sin\delta \qquad F_{xj,V} = F_{xj} \\ F_{yi,V} &= F_{xi}\sin\delta + F_{yi}\cos\delta \qquad F_{yj,V} = F_{yj} \end{aligned} \quad (21)$$

for $i \in \{1, 2\}$ and $j \in \{3, 4\}$

B. Tire and Slip Models

For the 3DOF model an extended tire brush model with combined slip was used [14] to model the tire forces. According to Pacejka [14], the longitudinal and lateral forces on a single tire are given by

$$F_x = F\frac{\sigma_x}{\sigma} \qquad F_y = F\frac{\sigma_y}{\sigma}, \quad (22)$$

where tire slip quantities σ, σ_x, and σ_y are obtained using the tire speed sensors and vehicle states obtained in section IV-A [14], and the magnitude of net force F is given by

$$F = \begin{cases} \mu F_z(3\theta_s\sigma - 3(\theta_s\sigma)^2 + (\theta_s\sigma)^3) & \text{if } \sigma \le \frac{1}{\theta_s} \\ \mu F_z & \text{if } \sigma \ge \frac{1}{\theta_s}, \end{cases} \quad (23)$$

where μ is the coefficient of friction of the road. F_z is the normal force on tire, and θ_s is a tire parameter defiined in [14]. Also, the tire aligning moment M_z is given by

$$M_z = -(t_p + t_m)F_y + cF_xF_y, \quad (24)$$

where t_p is the pneumatic trail of the tire defined in [14], c denotes carcass compliance, and t_m is the mechanical trail.

The vertical tire forces F_z for the road slope θ (lateral or longitudinal) are given by

$$F_z = \frac{mgl_r\cos\theta}{2(l_f + l_r)} \pm \Delta F_{z,roll} \pm \Delta F_{z,brake}, \quad (25)$$

where the force gradients $\Delta F_{z,brake}$ and $\Delta F_{z,roll}$ simulate the effects of braking and roll respectively and the signs of the force gradients depend on the location of the tire [14].

The steering rack force can then be obtained using the moments of front tires obtained using equation (24) as

$$F_R = i_p(M_{z1} + M_{z2}),$$

where i_p again defines the tire moment to rack force transmission ratio for the test vehicle. Apart from the common parameters specified in Table I, additional parameters required in the 3DOF model are specified in Table II.

Parameter	Value
h_1	0.55 m
h_2	0.05 m
$k_{\phi 1}$	2 kNms/rad
$k_{\phi 2}$	1.5 kNms/rad
t_f	0.8 m
t_r	0.79 m

Parameter	Value
I_{xx}	2500 kg m^2
I_{yy}	3200 kg m^2
I_{xz}	650 kg m^2
$c_{\phi 1}$	105 kNm/rad
$c_{\phi 2}$	55 kNm/rad
c	1.67×10^{-5} m/N

TABLE II: 3DOF model parameters

C. 3DOF Model Assembly

We now refer back to Fig. 1. The vehicle states, namely, lateral speed v, yaw rate $\dot{\psi}$, and roll angle ϕ are modeled using the vehicle model developed in section IV-A. The lateral speed v and yaw rate $\dot{\psi}$ are used to find tire speeds which in turn are used to determine the tire slip quantities [14]. The roll angle ϕ, along with the slope and speed inputs, determine the variations of normal force through equation

(25). Slip quantities and normal forces are used to find the tire forces and aligning moments using equations (23), (22) and (24). The tire forces and moments are finally converted to chassis forces using equation (21) and are fed back in the vehicle model in equations (15), (16), and (17) to generate states for the next time sample.

V. Experiment Design

To validate the performance of the 2DOF and 3DOF models for producing estimates of rack force, driving experiments were performed on a 2016 Lincoln MKX. The model-based estimates of rack force were compared to measurements from strain gauges installed on the rack in the test vehicle and to the estimates of a vehicle dynamics model available in the literature [1] referred to as the "Existing" model in this paper. During the driving manoeuvers, a rapid control prototyping platform (dSPACE MicroAutoBox) was used to link sensed steering angle and vehicle longitudinal velocity signals with an online simulation of the dynamic models (integrated in real-time Simulink), using CAN-bus communications at 250 Hz. The road slopes were estimated in real-time using longitudinal velocity, accelerometer, and yaw rate sensor readings coming from the CAN bus at 250 Hz. The accuracy of the slope estimation algorithm was checked using slope measurements from a high fidelity IMU (OXTS RT3003 v2) installed in the vehicle that transmitted signals at 100 Hz.

We used an experimental protocol in which driving manoeuvres resulted in large variation about nominal values for steering angle and lateral road slope while keeping the velocity constant. We then compared the performance of rack force estimation of the 2DOF model, the 3DOF model, and the Existing model. We found that in both manoeuvres, the 2DOF and 3DOF models had higher accuracies than the Existing model. Moreover, with aggressive steering inputs, the 3DOF model displayed higher accuracy than the 2DOF model. To elaborate these results, we present outcomes of the following two experiments:

1) Driving on a varying lateral slope with non-aggressive steering (Experiment 1)
2) Driving on a constant lateral slope with aggressive oscillatory steering (Experiment 2)

VI. Results and Discussion

Fig. 4 shows the graphs for Experiment 1. The inputs to the rack force model are shown in Fig. 4a, Fig. 4b, and Fig. 4c. The vehicle manoeuvre is depicted by three snapshots of the vehicle and road on the top of Fig. 4a. Fig. 4c shows the estimation accuracy of the slope estimation equation discussed in section II. The rack force estimates of the 2DOF model and the 3DOF model are presented in 4d and 4e respectively along with estimates of the Existing model and the measured rack force. Clearly both 2DOF and 3DOF models agree well with the sensor measurements and have higher accuracies than the Existing Model.

Inputs and results for Experiment 2 are shown in Fig. 5. This particular driving experiment was performed on a road with constant lateral slope of about 11°. As shown in

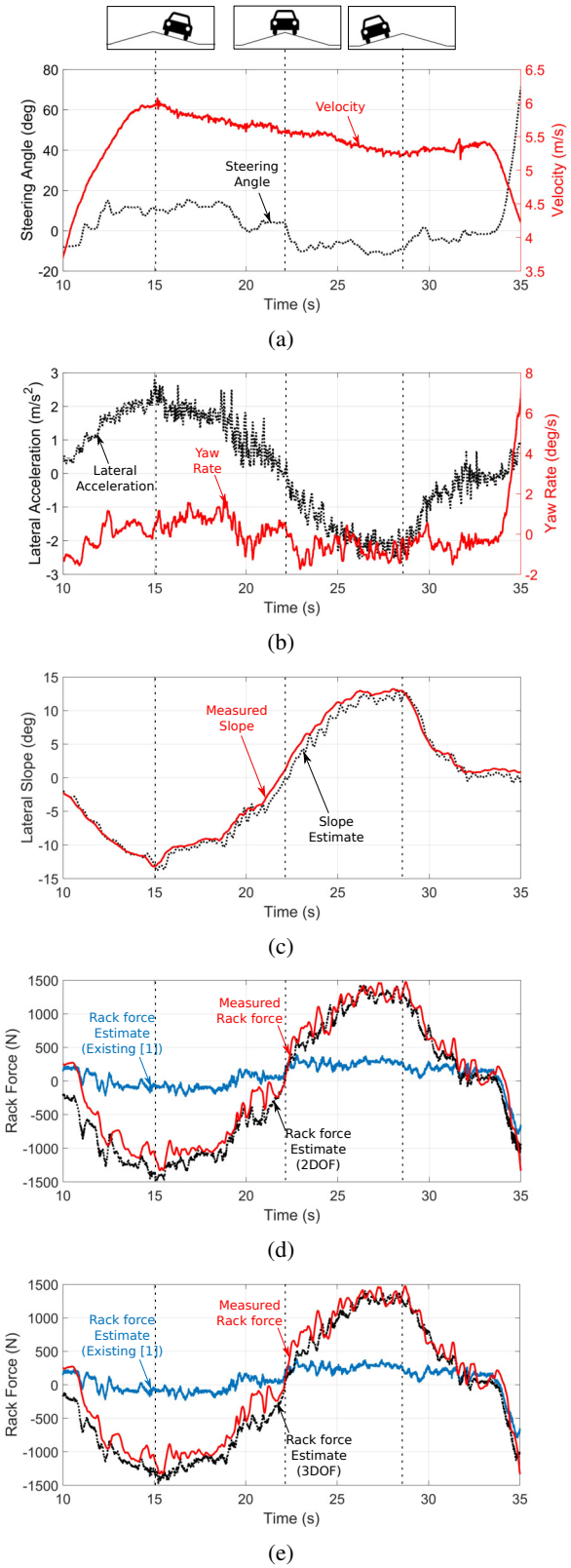

Fig. 4: Experiment 1 performed on a crowned road. (a) Inputs: non-aggressive steering angle and constant velocity (b) input lateral acceleration and yaw rate (c) Lateral slope estimated using equation (1) and measured using sensor (d) Rack force estimated using 2DOF model, Existing model, and measured using sensor (e) Rack force estimated using 3DOF model, Existing model, and measured using sensor.

Fig. 5a, the steering angle was varied aggressively between approximately $-60°$ and $60°$. Fig. 5b and Fig. 5c compare the accuracy of rack force estimates obtained using the 2DOF model and the 3DOF model with the estimates from Existing model and the sensor measurements. Again we see that both 2DOF and 3DOF models have higher accuracies than the Existing model. However, it is further seen that the rack force estimates obtained using the 3DOF model are more accurate than the estimates obtained using the 2DOF model.

The results from two experiments indicate that both 2DOF and 3DOF models perform better than the Existing model, and can therefore estimate the rack force due to road slopes which were ignored in the Existing model. Moreover, for normal steering maneuvers, the rack force estimates obtained using the 2DOF and 3DOF models are both highly accurate regardless of the magnitude and variation of the lateral road slope. However, for aggressive steering manoeuvres, the 3DOF model gives a more accurate rack force estimate than the 2DOF model. This can be due to a couple of reasons. First, the nonlinear tire model used in the 3DOF model might be better at capturing the tire slip and aligning moments for higher steering angles as compared to the linear tire model used in the 2DOF model. Second, the consideration of the effects of vehicle roll, load transfer, suspension parameters in the 3DOF model possibly improves the accuracy of state estimation and hence tire forces when compared with the 2DOF model in which such effects were neglected.

Future Work

In the future, we would like to analyze the robustness of our approach to parametric uncertainty especially in comparison with the estimation methods that are available in the literature. It would also be useful to identify the bandwidth of our rack force estimator to find the effectiveness of our method in different frequency ranges. Using our current modeling framework, we would also like to develop models that can estimate rack force due to certain other common road profile variations such as side-slopes and potholes. Finally, we would also like to explore the utility of our models in EPS controllers for improving the quality of steering feedback.

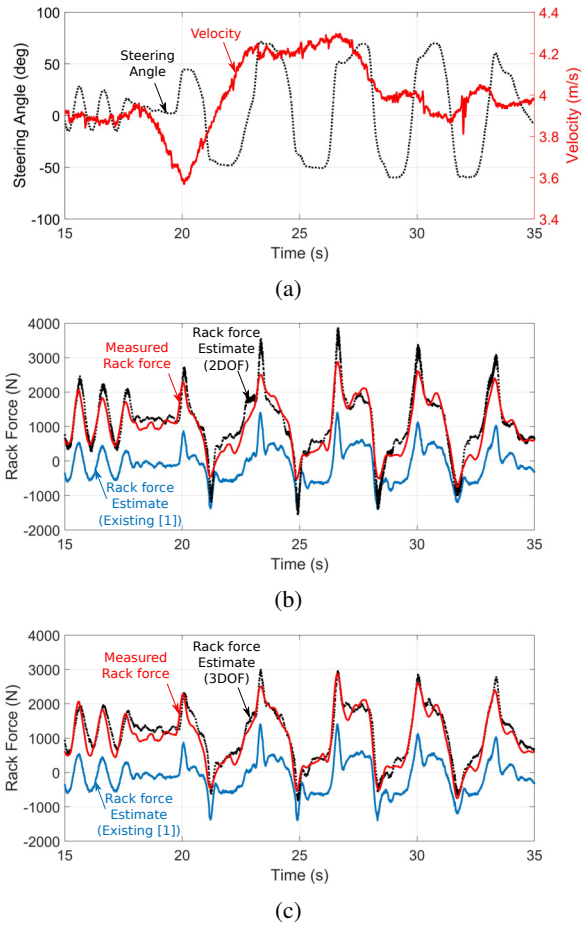

Fig. 5: Experiment 2 performed on road with constant slope. (a) Inputs: aggressive steering angle and constant velocity (b) Rack force estimated using 2DOF model, Existing model, and measured using sensor (c) Rack force estimated using 3DOF model, Existing model, and measured using sensor.

References

[1] J. Dornhege, S. Nolden, and M. Mayer, "Steering torque disturbance rejection," *SAE International Journal of Vehicle Dynamics, Stability, and NVH*, vol. 1, no. 2017-01-1482, pp. 165–172, 2017.

[2] S. Grüner, A. Gaedke, and G. G. Karch, "Control of electric power steering systems-from state of art to future challenges," in *Proceedings of the 17th World Congress The International Federation of Automatic Control*, pp. 10756–10757, 2008.

[3] A. J. Pick, T. J. Sworn, A. D. Barton, and J. O. P. Farrelly, "Rack force disturbance rejection," Sept. 25 2007. US Patent 7,273,127.

[4] J. M. Raad and D. Tuttle, "Pull-drift compensation enhancements," Aug. 5 2014. US Patent 8,798,865.

[5] S. Fankem, T. Weiskircher, and S. Müller, "Model-based rack force estimation for electric power steering," *IFAC Proceedings Volumes*, vol. 47, no. 3, pp. 8469–8474, 2014.

[6] M. Segawa, S. Nakano, M. Shino, and M. Nagai, "Preliminary study concerning quantitative analysis of steering system using hardware-in-the-loop (hil) simulator," tech. rep., SAE Technical Paper, 2006.

[7] L. Nehaoua, M. Djemai, and P. Pudlo, "Rack force feedback for an electrical power steering simulator," in *Control & Automation (MED), 2012 20th Mediterranean Conference on*, pp. 79–84, IEEE, 2012.

[8] M. A. Blommer, P. G. Sanders, H. E. Tseng, and D. Wang, "Systems and methods for decoupling steering rack force disturbances in electric steering," Apr. 3 2012. US Patent 8,150,582.

[9] D. Wang and F. Esser, "Epas system tests using rack force models," tech. rep., SAE Technical Paper, 2016.

[10] T. Weiskircher, S. Fankem, and B. Ayalew, "Rack force estimation for electric power steering," in *ASME 2015 International Design Engineering Technical Conferences and Computers and Information in Engineering Conference*, pp. V003T01A007–V003T01A007, American Society of Mechanical Engineers, 2015.

[11] T. Koch, *Untersuchungen zum Lenkgefühl von Steer-by-Wire Lenksystemen*. PhD thesis, Technische Universität München, 2010.

[12] S. R. Pastor and G. L. Tierney, "Method and apparatus for estimating incline and bank angles of a road surface," Aug. 29 1995. US Patent 5,446,658.

[13] A. Balachandran, S. M. Erlien, and J. C. Gerdes, "The virtual wheel concept for supportive steering feedback during active steering interventions," in *ASME 2014 Dynamic Systems and Control Conference*, pp. V002T27A005–V002T27A005, American Society of Mechanical Engineers, 2014.

[14] H. Pacejka, *Tire and vehicle dynamics*. Elsevier, 2005.

[15] H. E. Tseng, "Dynamic estimation of road bank angle," *Vehicle system dynamics*, vol. 36, no. 4-5, pp. 307–328, 2001.

[16] Y. Sebsadji, S. Glaser, S. Mammar, and J. Dakhlallah, "Road slope and vehicle dynamics estimation," in *American Control Conference, 2008*, pp. 4603–4608, IEEE, 2008.

[17] D. S. Bernstein, "Geometry, kinematics, statics, and dynamics," *Department of Aerospace Engineering, University of Michigan*, 2012.